11 Functional Renormalization Group Approach to Interacting Fermi Systems: DMFT as a Booster Rocket

Walter Metzner
Max Planck Institute for Solid State Research
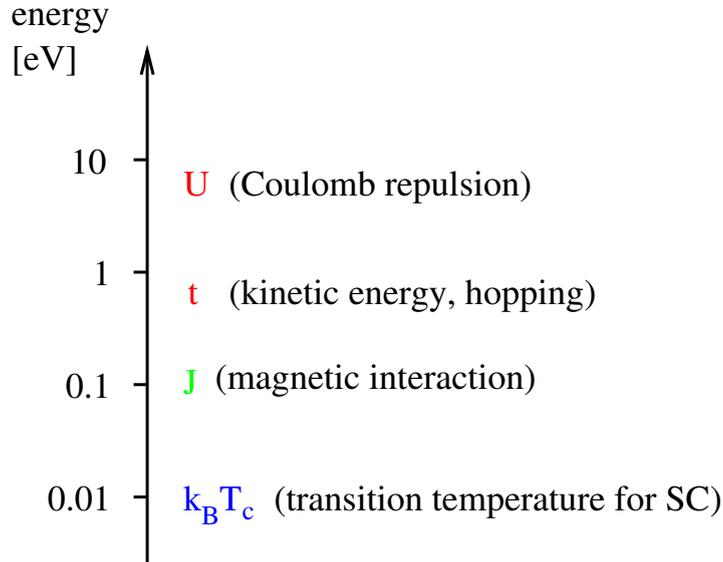Stuttgart

Contents

1   Introduction

Correlated electron compounds exhibit very distinct behavior on different energy and length scales. Collective phenomena emerge at scales far below the bare energy scales of the microscopic Hamiltonian. For example, in high-temperature superconductors one bridges three orders of magnitude from the highest scale, the bare Coulomb interaction, via the intermediate scale of short-range magnetic correlations, down to the lowest scale of d-wave superconductivity and other ordering phenomena (see Fig. 1). This diversity of scales is a major obstacle to a direct numerical solution of microscopic models, since the most interesting phenomena emerge only in large systems at low temperatures. It is also hard to tackle by conventional many-body methods if one tries to treat all scales at once and within the same approximation, for example by summing a subclass of Feynman diagrams. Perturbative approaches which do not separate different scales are plagued by infrared divergences and are therefore often inapplicable even at weak coupling.

It is thus natural to treat degrees of freedom with different energy or length scales step by step. This is the main idea behind all *renormalization group* (RG) schemes. Using a functional integral representation this strategy can be implemented by integrating out degrees of freedom (bosonic or fermionic fields) successively, following a suitable order of scales. One thus generates a one-parameter family of effective actions that interpolates smoothly between the bare action of the system, as given by the microscopic Hamiltonian, and the final effective action from which all physical properties can be extracted. The Green or vertex functions corresponding to the effective action at scale Λ obey a hierarchy of differential flow equations. This hierarchy is exact and involves the flow of functions of generally continuous variables. For these reasons this approach is frequently referred to as *"exact"* or *"functional"* RG [1–3].

The exact hierarchy can be solved exactly only in special cases, where the underlying model can also be solved exactly (and more easily) by other means. However, the functional RG is a valuable source for devising powerful new approximation schemes, which can be obtained by truncating the hierarchy and/or by a simplified parametrization of the Green or vertex functions. These approximations have several distinctive advantages: i) they have a renormalization group structure built in; that is, scales are handled successively and infrared singularities are thus treated properly; ii) they can be applied directly to microscopic models, not only to effective field theories that capture only some asymptotic behavior; iii) they are physically transparent; for example, one can see directly how and why new correlations form upon lowering the scale; iv) one can use different approximations at different scales. Small steps from a scale Λ to a slightly smaller scale Λ' are much easier to control than an integration over all degrees of freedom in one shot.

This lecture provides a concise introduction to the functional RG in the context of interacting Fermi systems. To illustrate the method at work, I review applications of the functional RG to the two-dimensional Hubbard model. A more detailed presentation and many other applications can be found in the recent review article Ref. [3]. In the last part I present the very recent idea [4] of using the DMFT solution as a non-perturbative starting point for a functional RG flow.

energy
[eV]

10 — U (Coulomb repulsion)

1 — t   (kinetic energy, hopping)

0.1 — J (magnetic interaction)

0.01 — $k_B T_c$ (transition temperature for SC)

Fig. 1: *Energy scales in cuprate high-temperature superconductors. Magnetic interactions and superconductivity are generated from the kinetic energy and the Coulomb repulsion. Figure taken from Ref. [3].*

2   Functional RG for Fermi systems

Already in the 1970s, various RG methods were used to deal with infrared singularities arising in one-dimensional Fermi systems [5]. Renormalization group approaches dealing with interacting fermions in higher dimensions were developed much later. Due to the extended (not point-like) geometry of the Fermi surface singularity in dimensions $d > 1$, the renormalization group flow cannot be reduced to a small number of running couplings, even if irrelevant interactions are discarded. Aiming at a mathematical control of interacting Fermi systems, Feldman and Trubowitz [6], and independently Benfatto and Gallavotti [7], formulated a rigorous fermionic version of Wilson's momentum-shell RG [8] for interacting fermions in dimensions $d > 1$. Important rigorous results for two-dimensional systems have indeed been obtained [9, 10]. An essential message from these results is that no hitherto unknown instabilities or non-perturbative effects occur in Fermi systems with sufficiently weak interactions, at least in the absence of special features such as van Hove singularities at the Fermi level.

The Wilsonian RG for interacting Fermi systems was popularized among physicists by Shankar [11] and Polchinski [12], who presented some of the main ideas in a pedagogical style. In particular, they discussed an intuitive RG perspective of Fermi liquid theory.

The Wilsonian RG is not only useful for a rigorous understanding of interacting fermion systems. A specific variant of Wilson's RG known as *exact* or *functional* RG turned out to provide a valuable framework for computational purposes. Approximations derived from exact functional flow equations play an increasingly important role in the theory of interacting Fermi systems [3]. Exact flow equations describe the evolution of a generating functional for all many-particle correlation or vertex functions as a function of a flow parameter Λ, usually a cutoff. They can be easily derived from a functional integral representation.

For computational purposes, the exact flow equation for the effective action Γ^Λ, first derived in the context of bosonic field theories by Wetterich [13], turned out to be most convenient. The effective action is the generating functional for one-particle irreducible vertex functions, which are obtained by taking derivatives with respect to the source fields. The flow parameter Λ describes a regularization of the bare action, which regularizes infrared divergencies in perturbation theory. The regularization is removed at the end of the flow, say for $\Lambda \to 0$. The initial regulator (for $\Lambda = \Lambda_0$) can be chosen such that Γ^{Λ_0} is given by the bare action. The flow of Γ^Λ then provides a smooth interpolation between the bare action of the system and the final effective action Γ, from which any desired information can be extracted. This flow is determined by an exact functional differential equation [13]. Expanding in the fields one obtains a hierarchy of flow equations for the one-particle irreducible vertex functions.

The expression *functional* RG stems from the feature that the exact flow equations describe the flow of a functional or (equivalently) of a hierarchy of functions. An important difference compared to Wilson's original formulation is that a complete set of source fields is kept in the flowing generating functionals, not only those corresponding to scales below Λ. Hence, the full information on the properties of the system remains accessible, not only the low energy or long wavelength behavior.

In the remainder of this section, I present the exact flow equations and their expansion in the source fields. The first subsection summarizes the standard functional integral formalism as described, for example, in the excellent textbook by Negele and Orland [14].

2.1 Generating functionals

A system of interacting fermions can be represented by Grassmann fields ψ, $\bar\psi$, and an action of the form

$$\mathcal{S}[\psi, \bar\psi] = -(\bar\psi, G_0^{-1}\psi) + V[\psi, \bar\psi] \,, \tag{1}$$

where $V[\psi, \bar\psi]$ is an arbitrary many-body interaction, and G_0 is the propagator of the non-interacting system. The bracket $(.,.)$ is a shorthand notation for the sum $\sum_K \bar\psi_K (G_0^{-1}\psi)_K$, where $(G_0^{-1}\psi)_K = \sum_{K'} G_0^{-1}(K, K') \psi_{K'}$. The Grassmann field index K collects the quantum numbers of a suitable single-particle basis set and the Matsubara frequency. The K-sums include integrals over continuous variables, and normalization factors such as temperature and volume. In particular, for spin-$1/2$ fermions with a single-particle basis labeled by momentum $\mathbf{k}$ and spin orientation σ, one has $K = (k_0, \mathbf{k}, \sigma)$, where k_0 is the fermionic Matsubara frequency. If the bare part of the action is translation and spin-rotation invariant, the bare propagator has the diagonal and spin-independent form $G_0(K, K') = \delta_{KK'} G_0(K)$ with

$$G_0(K) = \frac{1}{ik_0 - \xi_{\mathbf{k}}} \,, \tag{2}$$

where $\xi_{\mathbf{k}} = \epsilon_{\mathbf{k}} - \mu$ is the single-particle energy relative to the chemical potential. A two-particle interaction has the general form

$$V[\psi, \bar\psi] = \frac{1}{4} \sum_{K_1, K_2, K_1', K_2'} V(K_1', K_2'; K_1, K_2) \, \bar\psi_{K_1'} \bar\psi_{K_2'} \psi_{K_2} \psi_{K_1} \,. \tag{3}$$

The generating functional

$$\mathcal{G}[\eta, \bar{\eta}] = -\log \int \prod_K d\psi_K d\bar{\psi}_K \, e^{-\mathcal{S}[\psi, \bar{\psi}]} \, e^{(\bar{\eta}, \psi) + (\bar{\psi}, \eta)} \, , \tag{4}$$

yields connected m-particle *Green functions* via derivatives with respect to the source fields, that is,

$$G^{(2m)}(K_1, \ldots, K_m; K_1', \ldots, K_m') = -\langle \psi_{K_1} \ldots \psi_{K_m} \bar{\psi}_{K_m'} \ldots \bar{\psi}_{K_1'} \rangle_c$$

$$= (-1)^m \left. \frac{\partial^m}{\partial \bar{\eta}_{K_1} \ldots \partial \bar{\eta}_{K_m}} \frac{\partial^m}{\partial \eta_{K_m'} \ldots \partial \eta_{K_1'}} \mathcal{G}[\eta, \bar{\eta}] \right|_{\eta = \bar{\eta} = 0} \, , \tag{5}$$

where $\langle \ldots \rangle_c$ is the connected average of the product of Grassmann variables between the brackets. The one-particle Green function $G^{(2)}$ is the propagator of the interacting system, which is usually denoted without the superscript as G.

Legendre transforming $\mathcal{G}[\eta, \bar{\eta}]$ yields the *effective action*

$$\Gamma[\psi, \bar{\psi}] = (\bar{\eta}, \psi) + (\bar{\psi}, \eta) + \mathcal{G}[\eta, \bar{\eta}] \, , \tag{6}$$

where $\psi = -\partial \mathcal{G}/\partial \bar{\eta}$ and $\bar{\psi} = \partial \mathcal{G}/\partial \eta$. The effective action is the generating functional for one-particle irreducible *vertex functions*,

$$\Gamma^{(2m)}(K_1', \ldots, K_m'; K_1, \ldots, K_m) = \left. \frac{\partial^{2m} \Gamma[\psi, \bar{\psi}]}{\partial \bar{\psi}_{K_1'} \ldots \partial \bar{\psi}_{K_m'} \partial \psi_{K_m} \ldots \partial \psi_{K_1}} \right|_{\psi, \bar{\psi} = 0} \, . \tag{7}$$

The Legendre correspondence between the functionals $\mathcal{G}$ and Γ yields relations between the Green functions $G^{(2m)}$ and the vertex functions $\Gamma^{(2m)}$. In particular,

$$\Gamma^{(2)} = G^{-1} = G_0^{-1} - \Sigma \, , \tag{8}$$

where Σ is the self-energy. The two-particle Green function is related to the two-particle vertex by

$$G^{(4)}(K_1, K_2; K_1', K_2') = \sum_{P_1, P_2, P_1', P_2'} G(K_1, P_1') \, G(K_2, P_2')$$

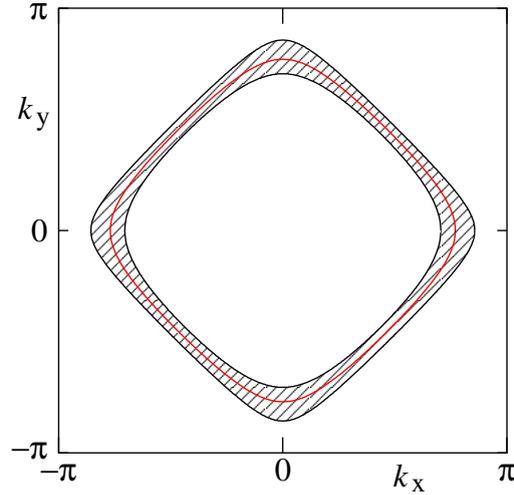$$\times \, \Gamma^{(4)}(P_1', P_2'; P_1, P_2) \, G(P_1, K_1') \, G(P_2, K_2') \, . \tag{9}$$

Generally, the m-particle Green functions are obtained by adding all trees that can be formed with vertex functions of equal or lower order and G-lines [14].

The effective action obeys the reciprocity relations

$$\frac{\partial \Gamma}{\partial \psi} = -\bar{\eta} \, , \quad \frac{\partial \Gamma}{\partial \bar{\psi}} = \eta \, . \tag{10}$$

The second functional derivatives of $\mathcal{G}$ and Γ with respect to the fields are also reciprocal. We define the matrices of second derivatives at *finite* fields

$$\mathbf{G}^{(2)}[\eta, \bar{\eta}] = \begin{pmatrix} -\dfrac{\partial^2 \mathcal{G}}{\partial \bar{\eta}_K \partial \eta_{K'}} & \dfrac{\partial^2 \mathcal{G}}{\partial \bar{\eta}_K \partial \bar{\eta}_{K'}} \\ \dfrac{\partial^2 \mathcal{G}}{\partial \eta_K \partial \eta_{K'}} & -\dfrac{\partial^2 \mathcal{G}}{\partial \eta_K \partial \bar{\eta}_{K'}} \end{pmatrix} = - \begin{pmatrix} \langle \psi_K \bar{\psi}_{K'} \rangle & \langle \psi_K \psi_{K'} \rangle \\ \langle \bar{\psi}_K \bar{\psi}_{K'} \rangle & \langle \bar{\psi}_K \psi_{K'} \rangle \end{pmatrix} \, , \tag{11}$$

Fig. 2: *Momentum space region around the Fermi surface excluded by a sharp momentum cutoff in a two-dimensional lattice fermion system. Figure taken from Ref. [3].*

and

$$
\mathbf{\Gamma}^{(2)}[\psi, \bar{\psi}] = \begin{pmatrix} \dfrac{\partial^2 \Gamma}{\partial \bar{\psi}_{K'} \partial \psi_K} & \dfrac{\partial^2 \Gamma}{\partial \bar{\psi}_{K'} \partial \bar{\psi}_K} \\ \dfrac{\partial^2 \Gamma}{\partial \psi_{K'} \partial \psi_K} & \dfrac{\partial^2 \Gamma}{\partial \psi_{K'} \partial \bar{\psi}_K} \end{pmatrix} , \tag{12}
$$

where the matrix elements in the second matrix of the last equation are just a more convenient notation for those in the first matrix. The reciprocity relation for the second derivatives reads

$$
\mathbf{\Gamma}^{(2)}[\psi, \bar{\psi}] = \left(\mathbf{G}^{(2)}[\eta, \bar{\eta}] \right)^{-1} . \tag{13}
$$

Note that *anomalous* components are involved as long as the source fields are finite. Only at $\eta = \bar{\eta} = 0$ and $\psi = \bar{\psi} = 0$, and in the absence of $U(1)$ charge symmetry breaking one has the simple relation $\Gamma^{(2)} = G^{-1}$.

2.2 Exact flow equation

We now endow the bare propagator G_0 with a dependence on a *flow parameter* Λ. Usually Λ is a cutoff suppressing contributions from fields with a single-particle energy or a Matsubara frequency below the scale Λ in the functional integral. For example, in a translation invariant system this may be done by modifying $G_0(K)$ to

$$
G_0^\Lambda(K) = \frac{\Theta^\Lambda(\mathbf{k})}{i k_0 - \xi_{\mathbf{k}}} , \tag{14}
$$

where $\Theta^\Lambda(\mathbf{k})$ is a function that vanishes for $|\xi_{\mathbf{k}}| \ll \Lambda$ and tends to one for $|\xi_{\mathbf{k}}| \gg \Lambda$. In this way the infrared singularity of the propagator at $k_0 = 0$ and $\xi_{\mathbf{k}} = 0$ is cut off at the scale Λ. The simplest choice for Θ^Λ is a step function, $\Theta^\Lambda(\mathbf{k}) = \Theta(|\xi_{\mathbf{k}}| - \Lambda)$, such that momenta in a shell around the Fermi surface are strictly excluded (see Fig. 2).

In the first applications of the functional RG to interacting Fermi systems a momentum cutoff was used, but later a frequency cutoff became more popular, since the latter does not interfere with Fermi surface shifts, and particle-hole excitations with a small momentum transfer are captured smoothly by the flow [15]. Moreover, a frequency cutoff can also be used in systems without translation invariance, such as systems with impurities [16].

The generating functionals constructed with G_0^Λ instead of G_0 depend on the flow parameter and will be denoted by $\mathcal{G}^\Lambda[\eta, \bar{\eta}]$ and $\Gamma^\Lambda[\psi, \bar{\psi}]$. The original functionals $\mathcal{G}$ and Γ are recovered in the limit $\Lambda \to 0$. The evolution of $\Gamma^\Lambda[\psi, \bar{\psi}]$ as a function of Λ is described by an *exact functional flow equation*,

$$\frac{d}{d\Lambda} \Gamma^\Lambda[\psi, \bar{\psi}] = -\left(\bar{\psi}, \partial_\Lambda Q_0^\Lambda \psi\right) - \frac{1}{2} \text{Tr} \left[\left(\partial_\Lambda \mathbf{Q}_0^\Lambda\right) \left(\mathbf{\Gamma}^{(2)\Lambda}[\psi, \bar{\psi}]\right)^{-1} \right] \, , \tag{15}$$

where

$$\mathbf{Q}_0^\Lambda = \begin{pmatrix} Q_0^\Lambda(K, K') & 0 \\ 0 & -Q_0^\Lambda(K', K) \end{pmatrix} \tag{16}$$

with $Q_0^\Lambda = (G_0^\Lambda)^{-1}$, and $\mathbf{\Gamma}^{(2)\Lambda}[\psi, \bar{\psi}]$ is the matrix of second derivatives of Γ^Λ at finite fields,

$$\mathbf{\Gamma}^{(2)\Lambda}[\psi, \bar{\psi}] = \begin{pmatrix} \dfrac{\partial^2 \Gamma^\Lambda}{\partial \bar{\psi}_K \partial \psi_{K'}} & \dfrac{\partial^2 \Gamma^\Lambda}{\partial \bar{\psi}_K \partial \bar{\psi}_{K'}} \\ \dfrac{\partial^2 \Gamma^\Lambda}{\partial \psi_K \partial \psi_{K'}} & \dfrac{\partial^2 \Gamma^\Lambda}{\partial \psi_K \partial \bar{\psi}_{K'}} \end{pmatrix} \, . \tag{17}$$

The trace on the right hand side of the flow equations includes a sum over the Grassmann field index K. Note that the inversion of $\mathbf{\Gamma}^{(2)\Lambda}[\psi, \bar{\psi}]$ in Eq. (15) is not merely an inversion of a 2×2 matrix, since it involves also the additional matrix structure coming from the dependence on the Grassmann field indices K and K'. A derivation of the functional flow equation (15) is presented in Appendix A.

Alternative definitions of the effective action Γ^Λ, differing by interaction-independent terms, have also been used. A frequently used variant is [1]

$$\Gamma_R^\Lambda[\psi, \bar{\psi}] = \Gamma^\Lambda[\psi, \bar{\psi}] + (\bar{\psi}, R^\Lambda \psi) \, , \tag{18}$$

where $R^\Lambda = Q_0^\Lambda - Q_0$. The additional quadratic term cancels the first term in the flow equation (15) for Γ^Λ, and one obtains the equivalent flow equation

$$\frac{d}{d\Lambda} \Gamma_R^\Lambda[\psi, \bar{\psi}] = -\frac{1}{2} \text{Tr} \left[\left(\partial_\Lambda \mathbf{R}^\Lambda\right) \left(\mathbf{\Gamma}_R^{(2)\Lambda}[\psi, \bar{\psi}] + \mathbf{R}^\Lambda\right)^{-1} \right] \, , \tag{19}$$

where $\mathbf{R}^\Lambda = \text{diag}\left(R^\Lambda(K, K'), -R^\Lambda(K', K)\right)$. The functional Γ_R^Λ and its anologue for bosonic fields is known as *effective average action* in the literature [1]. Both Γ_R^Λ and Γ^Λ tend to the same effective action Γ in the limit $\Lambda \to 0$, where R^Λ vanishes.

Choosing the initial cutoff Λ_0 such that $G_0^{\Lambda_0}$ is identically zero, all contributions to the functional integral are suppressed. For a sharp momentum cutoff this is achieved by choosing Λ_0 larger than $\max_{\mathbf{k}} |\xi_{\mathbf{k}}|$, while for a frequency cutoff one has to start with $\Lambda_0 = \infty$ to eliminate all

modes. At the initial scale Λ_0, one then has the simple initial condition $\Gamma_R^{\Lambda_0}[\psi, \bar{\psi}] = \mathcal{S}[\psi, \bar{\psi}]$, while

$$\Gamma^{\Lambda_0}[\psi, \bar{\psi}] = -(\bar{\psi}, Q_0^{\Lambda_0}\psi) + V[\psi, \bar{\psi}] = \mathcal{S}^{\Lambda_0}[\psi, \bar{\psi}] = \mathcal{S}[\psi, \bar{\psi}] - (\bar{\psi}, R^{\Lambda}\psi) . \tag{20}$$

Hence, Γ_R^{Λ} interpolates smoothly between the (unregularized) bare action $\mathcal{S}$ and the final effective action Γ, while Γ^{Λ} interpolates between the *regularized* bare action $\mathcal{S}^{\Lambda_0}$ and Γ. The initial "regularization" with $Q_0^{\Lambda_0} = \infty$ amounts to a complete suppression of all contributions to the functional integral, not just a regularization of divergent contributions.

2.3   Expansion in the fields

Expanding the functional flow equation (15) for the effective action in powers of the fields yields a hierarchy of flow equations for the m-particle vertex functions. To expand the inverse of $\mathbf{\Gamma}^{(2)\Lambda}[\psi, \bar{\psi}]$, we split

$$\mathbf{\Gamma}^{(2)\Lambda}[\psi, \bar{\psi}] = (\mathbf{G}^{\Lambda})^{-1} - \tilde{\mathbf{\Sigma}}^{\Lambda}[\psi, \bar{\psi}] , \tag{21}$$

where

$$\mathbf{G}^{\Lambda} = \left(\mathbf{\Gamma}^{(2)\Lambda}[\psi, \bar{\psi}] \big|_{\psi=\bar{\psi}=0} \right)^{-1} = \begin{pmatrix} G^{\Lambda}(K, K') & 0 \\ 0 & -G^{\Lambda}(K', K) \end{pmatrix} , \tag{22}$$

and $\tilde{\mathbf{\Sigma}}^{\Lambda}[\psi, \bar{\psi}]$ contains all contributions which are at least quadratic in the fields. Now the inverse of $\mathbf{\Gamma}^{(2)\Lambda}[\psi, \bar{\psi}]$ can be expanded in a geometric series,

$$\left(\mathbf{\Gamma}^{(2)\Lambda}[\psi, \bar{\psi}] \right)^{-1} = \left(1 - \mathbf{G}^{\Lambda}\tilde{\mathbf{\Sigma}}^{\Lambda}[\psi, \bar{\psi}] \right)^{-1} \mathbf{G}^{\Lambda}$$
$$= \left[1 + \mathbf{G}^{\Lambda}\tilde{\mathbf{\Sigma}}^{\Lambda}[\psi, \bar{\psi}] + (\mathbf{G}^{\Lambda}\tilde{\mathbf{\Sigma}}^{\Lambda}[\psi, \bar{\psi}])^2 + \dots \right] \mathbf{G}^{\Lambda} . \tag{23}$$

Inserting this into the functional flow equation yields

$$\frac{d}{d\Lambda}\Gamma^{\Lambda}[\psi, \bar{\psi}] = - \operatorname{Tr}\left[(\partial_{\Lambda}Q_0^{\Lambda})G^{\Lambda}\right] - \left(\bar{\psi}, \partial_{\Lambda}Q_0^{\Lambda}\psi\right)$$
$$+ \frac{1}{2}\operatorname{Tr}\left[\mathbf{S}^{\Lambda}(\tilde{\mathbf{\Sigma}}^{\Lambda}[\psi, \bar{\psi}] + \tilde{\mathbf{\Sigma}}^{\Lambda}[\psi, \bar{\psi}]\mathbf{G}^{\Lambda}\tilde{\mathbf{\Sigma}}^{\Lambda}[\psi, \bar{\psi}] + \dots)\right] , \tag{24}$$

with the *single scale propagator*

$$\mathbf{S}^{\Lambda} = -\mathbf{G}^{\Lambda}\left(\partial_{\Lambda}\mathbf{Q}_0^{\Lambda}\right)\mathbf{G}^{\Lambda} = \frac{d}{d\Lambda}\mathbf{G}^{\Lambda}\big|_{\mathbf{\Sigma}^{\Lambda} \text{ fixed}} . \tag{25}$$

The latter usually has its main support *at* the scale Λ. For example, for a sharp momentum cutoff acting on $\xi_{\mathbf{k}}$ as in Eq. (14), $\mathbf{S}^{\Lambda}$ has a delta-peak at $|\xi_{\mathbf{k}}| = \Lambda$ and vanishes elsewhere. Expanding $\Gamma^{\Lambda}[\psi, \bar{\psi}]$ and $\tilde{\mathbf{\Sigma}}^{\Lambda}[\psi, \bar{\psi}]$ in powers of ψ and $\bar{\psi}$, and comparing coefficients in Eq. (24), one obtains the flow equations for the self-energy $\Sigma^{\Lambda} = Q_0^{\Lambda} - \Gamma^{(2)\Lambda}$, the two-particle vertex $\Gamma^{(4)\Lambda}$, and all other m-particle vertices. The first three equations of this hierarchy are represented diagrammatically in Fig. 3. Note that only one-particle irreducible one-loop diagrams contribute, and internal lines are dressed by the self-energy. Contributions with several loops

Fig. 3: *Diagrammatic representation of the flow equations for the self-energy, the two-particle vertex, and the three-particle vertex. Lines with a dash correspond to the single-scale propagator S^Λ, and the other lines to the full propagator G^Λ. Figure taken from Ref. [3].*

are generated only indirectly upon inserting the flow of higher order vertices into lower order flow equations. The flow equation for the self-energy has the simple form

$$\frac{d}{d\Lambda}\Sigma^\Lambda(K',K) = \sum_{P,P'} S^\Lambda(P,P')\,\Gamma^{(4)\Lambda}(K',P';K,P)\,. \tag{26}$$

The flow equation for the two-particle vertex reads

$$\frac{d}{d\Lambda}\Gamma^{(4)\Lambda}(K'_1,K'_2;K_1,K_2) = -\sum_{P_1,P'_1}\sum_{P_2,P'_2} G^\Lambda(P_1,P'_1)\,S^\Lambda(P_2,P'_2)$$

$$\times\left\{\Gamma^{(4)\Lambda}(K'_1,K'_2;P_1,P_2)\Gamma^{(4)\Lambda}(P'_1,P'_2;K_1,K_2)\right.$$

$$-\left[\Gamma^{(4)\Lambda}(K'_1,P'_2;K_1,P_1)\Gamma^{(4)\Lambda}(P'_1,K'_2;P_2,K_2) + (P_1\leftrightarrow P_2,P'_1\leftrightarrow P'_2)\right]$$

$$+\left.\left[\Gamma^{(4)\Lambda}(K'_2,P'_2;K_1,P_1)\Gamma^{(4)\Lambda}(P'_1,K'_1;P_2,K_2) + (P_1\leftrightarrow P_2,P'_1\leftrightarrow P'_2)\right]\right\}$$

$$-\sum_{P,P'} S^\Lambda(P,P')\,\Gamma^{(6)\Lambda}(K'_1,K'_2,P';K_1,K_2,P)\,. \tag{27}$$

There are several contributions that are quadratic in $\Gamma^{(4)\Lambda}$, corresponding to the particle-particle, direct particle-hole, and crossed particle-hole channel, respectively.

The one-particle irreducibility is a convenient feature of flow equations derived from the effective action $\Gamma^\Lambda[\psi,\bar\psi]$. Flow equations derived from other functionals, such as the Polchinski equations [17] and their Wick ordered variant [9], contain also one-particle reducible contributions.
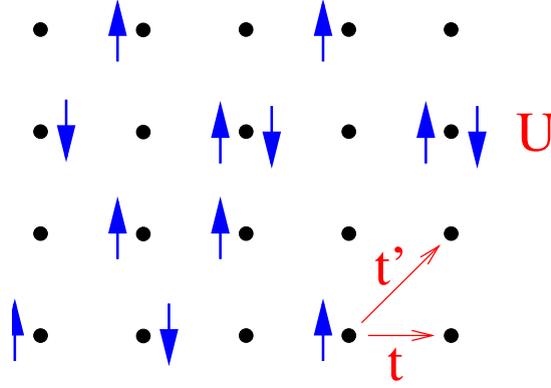
Fig. 4: *Hubbard model with nearest and next-to-nearest neighbor hopping on a square lattice.*

The full hierarchy of flow equations does not close at any finite order, since the flow of each $\Gamma^{(2m)\Lambda}$ receives a contribution from a tadpole diagram with $\Gamma^{(2m+2)\Lambda}$. Exact solutions of the flow equation hierarchy are possible only for relatively simple models, such as the Luttinger model [18], the reduced BCS model [19], or other mean-field models [20, 21], which can also be solved more directly by other methods. Usually the hierarchy of flow equations has to be truncated by neglecting effective interactions of higher order, and by using a simplified parametrization of the functional dependence of the remaining interactions on momenta, frequencies, et cetera. Truncations of the hierarchy at some finite order can be justified in case of sufficiently weak interactions, or if higher order terms are suppressed due to small phase space volumina [22]. Geometrical phase space restrictions are typically stronger in multi-loop integrals. A simplified parametrization of effective interactions can be obtained by neglecting dependences which become irrelevant in the low-energy limit.

3 Two-dimensional Hubbard model

Shortly after the discovery of high-temperature superconductivity in several cuprate compounds, Anderson [23] pointed out that the essential physics of the electrons in the copper-oxide planes of these materials could be described by the two-dimensional Hubbard model. The model describes tight-binding electrons with inter-site hopping amplitudes $t_{\mathbf{ij}}$ and a local repulsion $U > 0$, as specified by the Hamiltonian (see also Fig. 4)

$$H = \sum_{\mathbf{i,j}} \sum_{\sigma} t_{\mathbf{ij}}\, c_{\mathbf{i}\sigma}^{\dagger} c_{\mathbf{j}\sigma} + U \sum_{\mathbf{j}} n_{\mathbf{j}\uparrow} n_{\mathbf{j}\downarrow} \, . \tag{28}$$

Here $c_{\mathbf{i}\sigma}^{\dagger}$ and $c_{\mathbf{i}\sigma}$ are creation and annihilation operators for spin-$1/2$ fermions with spin orientation σ on a lattice site $\mathbf{i}$, and $n_{\mathbf{j}\sigma} = c_{\mathbf{j}\sigma}^{\dagger} c_{\mathbf{j}\sigma}$. The number of lattice sites will be denoted by L. A hopping amplitude $-t$ between nearest neighbors and an amplitude $-t'$ between next-nearest neighbors on a square lattice leads to the dispersion relation

$$\epsilon_{\mathbf{k}} = -2t(\cos k_x + \cos k_y) - 4t'(\cos k_x \, \cos k_y) \tag{29}$$
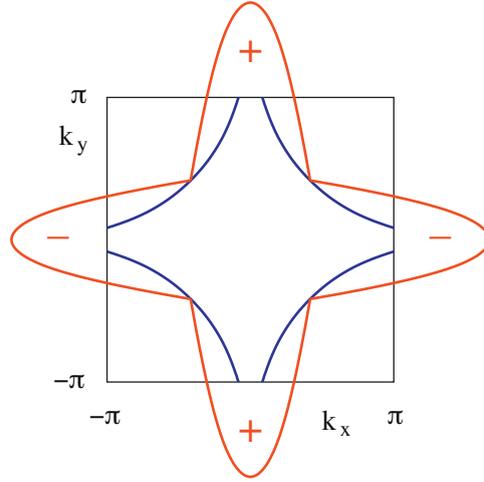
Fig. 5: *Schematic shape of the gap function $\Delta_{\mathbf{k}}$ with $d_{x^2-y^2}$-wave symmetry, for $\mathbf{k}$ tracing the Fermi surface.*

for single-particle states. This dispersion relation has saddle points at $\mathbf{k} = (0, \pi)$ and $(\pi, 0)$, which entail logarithmic van Hove singularities in the non-interacting density of states at the energy $\epsilon_{\mathrm{vH}} = 4t'$.

In agreement with the generic phase diagram of the cuprates, the Hubbard model exhibits antiferromagnetic order at half-filling, and has been expected to become a d-wave superconductor away from half-filling in two dimensions for quite some time [24]. The exchange of antiferromagnetic spin fluctuations has been proposed as a plausible mechanism leading to d-wave pairing [25–27]. In this picture, the BCS effective interaction $V_{\mathbf{k}\mathbf{k}'}$ is roughly proportional to the spin correlation function $\chi_s(\mathbf{k}-\mathbf{k}')$. Close to half-filling, $\chi_s(\mathbf{q})$ has a pronounced maximum at or near the antiferromagnetic wave vector (π, π). As a consequence, the BCS gap equation

$$\Delta_{\mathbf{k}} = -\int \frac{d^2\mathbf{k}'}{(2\pi)^2} V_{\mathbf{k}\mathbf{k}'} \frac{\Delta_{\mathbf{k}'}}{2E_{\mathbf{k}'}} \tag{30}$$

with $E_{\mathbf{k}} = (\xi_{\mathbf{k}}^2 + |\Delta_{\mathbf{k}}|^2)^{1/2}$ has a solution with $d_{x^2-y^2}$-wave symmetry such that the gap $\Delta_{\mathbf{k}}$ has maximal modulus but opposite sign near the points $(\pi, 0)$ and $(0, \pi)$ in the Brillouin zone [24], as illustrated in Fig. 5. This intuitive argument has been corroborated by a self-consistent perturbative solution of the two-dimensional Hubbard model within the so-called fluctuation-exchange approximation [28, 29].

The spin-fluctuation mechanism for pairing might be spoiled by other contributions to the BCS interactions and also by spin density wave instabilities. It turned out to be very hard to detect superconductivity in the Hubbard model by exact numerical computation [24, 30] as a consequence of finite size and/or temperature limitations. Fortunately, the tendency toward antiferromagnetism and d-wave pairing is already captured by the two-dimensional Hubbard model at *weak* coupling. Conventional perturbation theory breaks down for densities close to half-filling, since competing infrared divergences appear as a consequence of Fermi surface nesting and van Hove singularities. A controlled and unbiased treatment of these divergences is achieved by a renormalization group analysis, which takes into account the particle-particle and particle-hole channels on equal footing.

Early RG studies of the two-dimensional Hubbard model started with simple scaling approaches, very shortly after the discovery of high-T_c superconductivity [31–33]. These studies focused on dominant scattering processes between the van Hove points in **k**-space, for which a small number of running couplings could be defined and computed on a one-loop level. Spin-density and superconducting instabilities were identified from divergences of the corresponding correlation functions.

A complete treatment of all scattering processes in the Brillouin zone is more complicated since the effective interactions cannot be parametrized accurately by a small number of variables, even if irrelevant momentum and energy dependences are neglected. The *tangential* momentum dependence of effective interactions along the Fermi surface is strong and important in the low-energy limit. Hence, one has to deal with the renormalization of *functions*. This problem is treated most naturally by the functional RG.

3.1 Stability analysis at weak coupling

To detect instabilities in the weak-coupling limit, one can truncate the infinite hierarchy of flow equations at second order in the effective two-particle interaction and discard all vertices of higher order, and also self-energy corrections. The flow of the two-particle vertex is then fully determined by the first contribution in the second line of Fig. 3. In the absence of self-energy corrections, the internal lines are given by the bare propagator G_0^Λ and its scale derivative $S_0^\Lambda = \frac{d}{d\Lambda} G_0^\Lambda$.

Due to translation invariance on the lattice, G_0^Λ is diagonal in the momentum representation, that is, $G_0^\Lambda(K, K') = \delta_{KK'} G_0^\Lambda(K)$, where $K = (k, \sigma)$ with $k = (k_0, \mathbf{k})$. Hence, the truncated (without $\Gamma^{(6)\Lambda}$) flow equation (27) for the two-particle vertex can be written as

$$
\begin{aligned}
\frac{d}{d\Lambda} \Gamma^\Lambda(K_1', K_2'; K_1, K_2) \;=\; & -\frac{1}{\beta L} \sum_{P,P'} \frac{d}{d\Lambda} \left[G_0^\Lambda(P)\, G_0^\Lambda(P') \right] \\
\times \; & \Bigg[\frac{1}{2} \Gamma^\Lambda(K_1', K_2'; P, P')\, \Gamma^\Lambda(P, P'; K_1, K_2) \\
& - \Gamma^\Lambda(K_1', P'; K_1, P)\, \Gamma^\Lambda(P, K_2'; P', K_2) \\
& + \Gamma^\Lambda(K_2', P'; K_1, P)\, \Gamma^\Lambda(P, K_1'; P', K_2) \Bigg] .
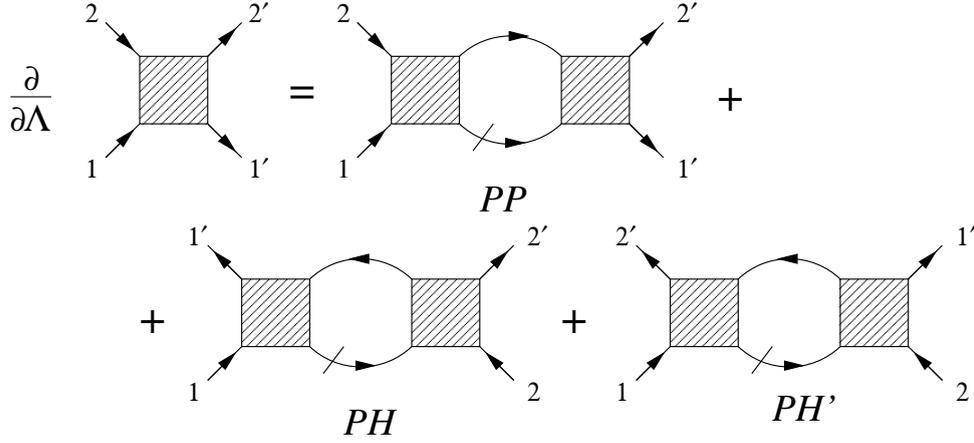\end{aligned}
\tag{31}
$$

Here and in the following, we denote the two-particle vertex as Γ^Λ, and we now write temperature ($\beta = 1/T$) and volume factors explicitly. The three terms on the right-hand side correspond to the particle-particle (PP), the direct particle-hole (PH) and the crossed particle-hole (PH') channel, respectively, see Fig. 6.

Due to spin rotation invariance, the spin structure of the two-particle vertex is relatively simple. One can express the vertex by a single function V^Λ depending only on momenta and Matsubara frequencies [22],

$$
\Gamma^\Lambda(K_1', K_2'; K_1, K_2) = V^\Lambda(k_1', k_2'; k_1, k_2)\, \delta_{\sigma_1 \sigma_{1'}} \delta_{\sigma_2 \sigma_{2'}} - V^\Lambda(k_2', k_1'; k_1, k_2)\, \delta_{\sigma_1 \sigma_{2'}} \delta_{\sigma_2 \sigma_{1'}} .
\tag{32}
$$

Alternatively, one may decompose the vertex in singlet and triplet components [34],

$$
\Gamma^\Lambda(K_1', K_2'; K_1, K_2) = \Gamma_s^\Lambda(k_1', k_2'; k_1, k_2)\, S_{\sigma_1', \sigma_2'; \sigma_1, \sigma_2} + \Gamma_t^\Lambda(k_1', k_2'; k_1, k_2)\, T_{\sigma_1', \sigma_2'; \sigma_1, \sigma_2} ,
\tag{33}
$$

Fig. 6: *One-loop flow equation for the two-particle vertex Γ^Λ with the particle-particle channel (PP) and the two particle-hole channels (PH and PH') written explicitly.*

where

$$
\begin{aligned}
S_{\sigma_1',\sigma_2';\sigma_1,\sigma_2} &= \tfrac{1}{2}\left(\delta_{\sigma_1\sigma_1'}\delta_{\sigma_2\sigma_2'} - \delta_{\sigma_1\sigma_2'}\delta_{\sigma_2\sigma_1'}\right), \\
T_{\sigma_1',\sigma_2';\sigma_1,\sigma_2} &= \tfrac{1}{2}\left(\delta_{\sigma_1\sigma_1'}\delta_{\sigma_2\sigma_2'} + \delta_{\sigma_1\sigma_2'}\delta_{\sigma_2\sigma_1'}\right).
\end{aligned}
\tag{34}
$$

Of course, one can easily compute Γ_s^Λ and Γ_t^Λ from V^Λ and vice versa [21]. The singlet vertex is symmetric, and the triplet vertex is antisymmetric under exchanges $k_1 \leftrightarrow k_2$ or $k_1' \leftrightarrow k_2'$.

We now outline the steps made to cast the one-loop flow equations in a form amenable to a numerical solution. To be specific, we use the singlet-triplet decomposition of the vertex and a momentum cutoff. Carrying out the spin sum in the flow equation one obtains

$$
\begin{aligned}
\partial_\Lambda \Gamma_\alpha^\Lambda(k_1', k_2'; k_1, k_2) = -\sum_{i=s,t}\sum_{j=s,t} & \left[C_{\alpha ij}^{\mathrm{PP}} \beta_{ij}^{\mathrm{PP}}(k_1', k_2'; k_1, k_2) \right. \\
& \left. + C_{\alpha ij}^{\mathrm{PH}} \beta_{ij}^{\mathrm{PH}}(k_1', k_2'; k_1, k_2) + C_{\alpha ij}^{\mathrm{PH'}} \beta_{ij}^{\mathrm{PH'}}(k_1', k_2'; k_1, k_2) \right]
\end{aligned}
\tag{35}
$$

for $\alpha = s, t$, where $C_{\alpha ij}^{\mathrm{PP}}$ etc. are simple numerical coefficients [34] and

$$
\beta_{ij}^{\mathrm{PP}}(k_1', k_2'; k_1, k_2) = \frac{1}{2\beta L}\sum_{k,k'}\partial_\Lambda\left[G_0^\Lambda(k)\,G_0^\Lambda(k')\right]\Gamma_i^\Lambda(k_1', k_2'; k, k')\,\Gamma_j^\Lambda(k, k'; k_1, k_2),
$$

$$
\beta_{ij}^{\mathrm{PH}}(k_1', k_2'; k_1, k_2) = -\frac{1}{\beta L}\sum_{k,k'}\partial_\Lambda\left[G_0^\Lambda(k)\,G_0^\Lambda(k')\right]\Gamma_i^\Lambda(k_1', k; k_1, k')\,\Gamma_j^\Lambda(k', k_2'; k, k_2),
$$

$$
\beta_{ij}^{\mathrm{PH'}}(k_1', k_2'; k_1, k_2) = -\beta_{ij}^{\mathrm{PH}}(k_2', k_1'; k_1, k_2).
\tag{36}
$$

It is clearly impossible to solve the flow equations with the full energy and momentum dependence of the vertex function, since Γ^Λ has three independent energy and momentum variables. However, the flow equations can be simplified considerably by ignoring dependences which are irrelevant (in the RG sense) in the low-energy limit, that is, the energy dependence and the momentum dependence normal to the Fermi surface [3, 11].

Neglecting the energy dependence, we approximate

$$\Gamma_\alpha^\Lambda(k_1', k_2'; k_1, k_2) \approx \Gamma_\alpha^\Lambda(\mathbf{k}_1', \mathbf{k}_2'; \mathbf{k}_1, \mathbf{k}_2) \ . \tag{37}$$

Choosing an energy independent cutoff function $\Theta^\Lambda(\mathbf{k})$ as in Eq. (14), the Matsubara sums on the right hand side of the flow equations can be performed analytically, yielding

$$\partial_\Lambda \Gamma_\alpha^\Lambda(\mathbf{k}_1', \mathbf{k}_2'; \mathbf{k}_1, \mathbf{k}_2) = -\sum_{i=s,t} \sum_{j=s,t} \big[C_{\alpha ij}^{\mathrm{PP}} \beta_{ij}^{\mathrm{PP}}(\mathbf{k}_1', \mathbf{k}_2'; \mathbf{k}_1, \mathbf{k}_2)$$
$$+ C_{\alpha ij}^{\mathrm{PH}} \beta_{ij}^{\mathrm{PH}}(\mathbf{k}_1', \mathbf{k}_2'; \mathbf{k}_1, \mathbf{k}_2) + C_{\alpha ij}^{\mathrm{PH}'} \beta_{ij}^{\mathrm{PH}'}(\mathbf{k}_1', \mathbf{k}_2'; \mathbf{k}_1, \mathbf{k}_2) \big] \tag{38}$$

for $\alpha = s, t$, where the β-functions are now energy independent and read

$$\beta_{ij}^{\mathrm{PP}}(\mathbf{k}_1', \mathbf{k}_2'; \mathbf{k}_1, \mathbf{k}_2) = \frac{1}{2L} \sum_{\mathbf{k},\mathbf{k}'} \partial_\Lambda \big[\Theta^\Lambda(\mathbf{k})\, \Theta^\Lambda(\mathbf{k}') \big]$$
$$\times \frac{f(-\xi_\mathbf{k}) - f(\xi_{\mathbf{k}'})}{\xi_\mathbf{k} + \xi_{\mathbf{k}'}} \Gamma_i^\Lambda(\mathbf{k}_1', \mathbf{k}_2'; \mathbf{k}, \mathbf{k}')\, \Gamma_j^\Lambda(\mathbf{k}, \mathbf{k}'; \mathbf{k}_1, \mathbf{k}_2) \ ,$$

$$\beta_{ij}^{\mathrm{PH}}(\mathbf{k}_1', \mathbf{k}_2'; \mathbf{k}_1, \mathbf{k}_2) = -\frac{1}{L} \sum_{\mathbf{k},\mathbf{k}'} \partial_\Lambda \big[\Theta^\Lambda(\mathbf{k})\, \Theta^\Lambda(\mathbf{k}') \big]$$
$$\times \frac{f(\xi_\mathbf{k}) - f(\xi_{\mathbf{k}'})}{\xi_\mathbf{k} - \xi_{\mathbf{k}'}} \Gamma_i^\Lambda(\mathbf{k}_1', \mathbf{k}; \mathbf{k}_1, \mathbf{k}')\, \Gamma_j^\Lambda(\mathbf{k}', \mathbf{k}_2'; \mathbf{k}, \mathbf{k}_2) \ ,$$

$$\beta_{ij}^{\mathrm{PH}'}(\mathbf{k}_1', \mathbf{k}_2'; \mathbf{k}_1, \mathbf{k}_2) = -\beta_{ij}^{\mathrm{PH}}(\mathbf{k}_2', \mathbf{k}_1'; \mathbf{k}_1, \mathbf{k}_2) \ , \tag{39}$$

with the Fermi function $f(\xi) = \big[e^{\beta\xi} + 1 \big]^{-1}$. Note that momentum conservation implies that $\mathbf{k}$ and $\mathbf{k}'$ are related by $\mathbf{k} + \mathbf{k}' = \mathbf{k}_1 + \mathbf{k}_2$ in the particle-particle channel and by $\mathbf{k} + \mathbf{k}_1' = \mathbf{k}' + \mathbf{k}_1$ in the direct particle-hole channel. Hence, only one independent momentum variable needs to be summed. For a sharp momentum cutoff $\Theta^\Lambda(\mathbf{k}) = \Theta(|\xi_\mathbf{k}| - \Lambda)$ one has $\partial_\Lambda \Theta^\Lambda(\mathbf{k}) = -\delta(|\xi_\mathbf{k}| - \Lambda)$, so that the two-dimensional momentum integral can be reduced to a one-dimensional integral. The flow equation can be solved only if the momentum dependence of the vertex function is simplified. At least for weak coupling (in practice also for moderate ones), the vertex function acquires strong momentum dependences only for momenta close to the Fermi surface. Note that for the Hubbard model the bare vertex function Γ^{Λ_0} does not depend on momentum at all. Weak coupling instabilities are signalled by divergencies of the vertex function Γ^Λ, which are driven by momenta close to the Fermi surface. Hence, we will focus on the flow of the vertex function with momenta close to the Fermi surface. For arbitrary momenta, we approximate the vertex by

$$\Gamma_\alpha^\Lambda(\mathbf{k}_1', \mathbf{k}_2'; \mathbf{k}_1, \mathbf{k}_2) \approx \Gamma_\alpha^\Lambda(\mathbf{k}_{F1}', \mathbf{k}_{F1} + \mathbf{k}_{F2} - \mathbf{k}_{F1}'; \mathbf{k}_{F1}, \mathbf{k}_{F2}) \tag{40}$$

where $\mathbf{k}_{F1}$ etc. are projections of $\mathbf{k}_1$ etc. on the Fermi surface (see Fig. 7). Strong momentum dependences of the effective vertex are built up only by contributions with intermediate momenta $\mathbf{k}$ and $\mathbf{k}'$ (on the right hand side of the flow equations) which are close to the Fermi surface, because for such momenta the ratios $\frac{f(\mp\xi_\mathbf{k}) - f(\xi_{\mathbf{k}'})}{\xi_\mathbf{k} \pm \xi_{\mathbf{k}'}}$ in Eq. (39) can be big. Hence, for the most important momenta, the error made by the projection is relatively small (even if Λ
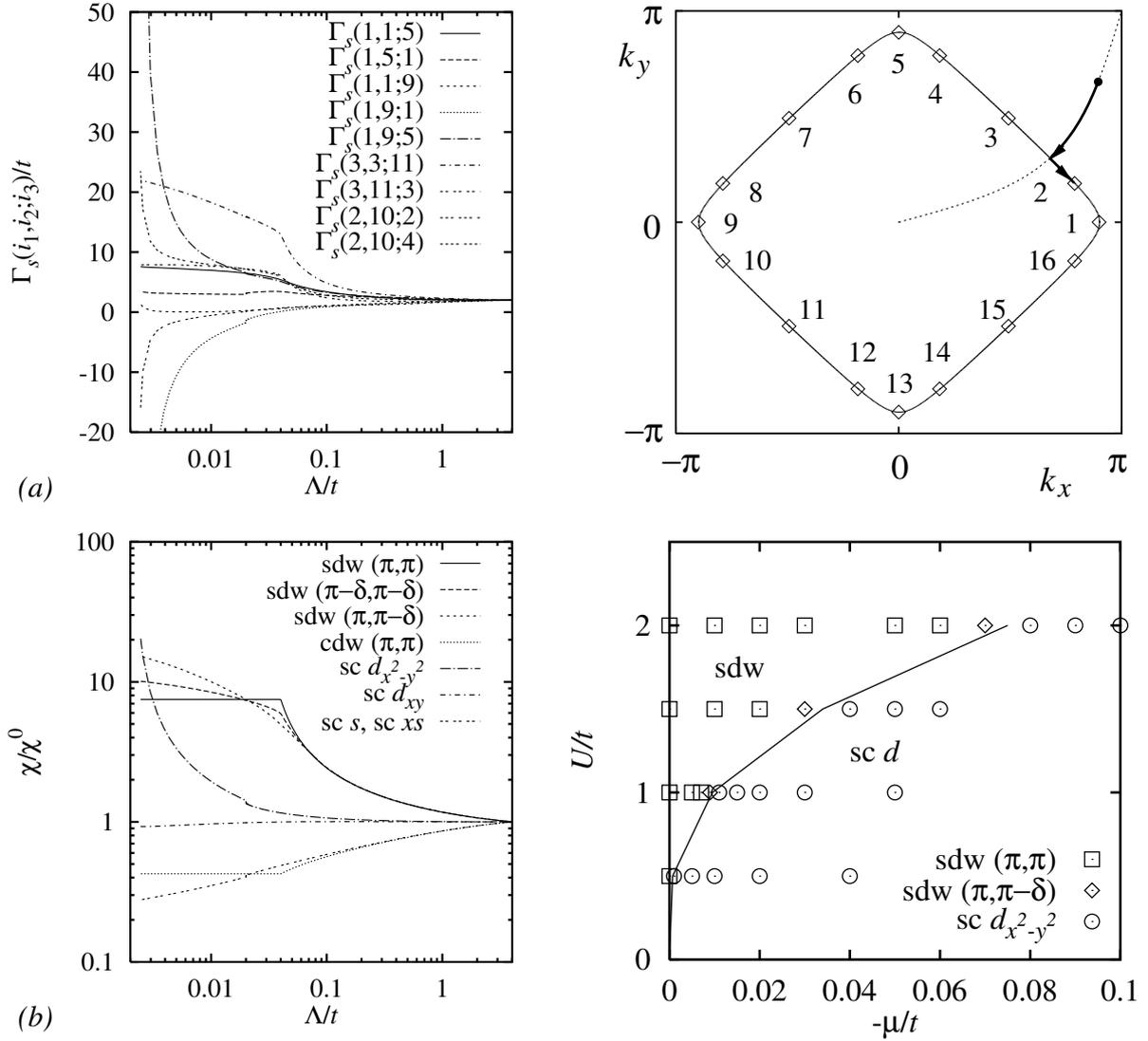
Fig. 7: *(a) Flow of the singlet component of the two-particle vertex Γ_s^Λ as a function of Λ for several choices of the Fermi momenta $\mathbf{k}_{F1}$, $\mathbf{k}_{F2}$ and $\mathbf{k}'_{F1}$, which are labeled according to the projection in the figure on the right. The model parameters are $U = t$ and $t' = 0$, the chemical potential is $\mu = -0.02t$, and the temperature is zero. (b) Left: Flow of the ratio of interacting and non-interacting susceptibilities, $\chi^\Lambda/\chi_0^\Lambda$, for the same parameters as in (a). Right: Ground state phase diagram for $t' = 0$ and $\mu \leq 0$ (at and below half-filling), as obtained from divergent susceptibilities. Figures taken from Ref. [34].*

is not small), because these momenta are close to their projected counterparts. The projected vertex function can be parameterized by three angles ϕ_1, ϕ_2, ϕ_3 associated with $\mathbf{k}_{F1}$, $\mathbf{k}_{F2}$ and $\mathbf{k}'_{F1}$, respectively, i.e.

$$\Gamma_\alpha^\Lambda(\mathbf{k}'_{F1}, \mathbf{k}_{F1} + \mathbf{k}_{F2} - \mathbf{k}'_{F1}; \mathbf{k}_{F1}, \mathbf{k}_{F2}) = \Gamma_\alpha^\Lambda(\phi_1, \phi_2, \phi_3) \tag{41}$$

The angular dependence turns out to be strong for small Λ and cannot be neglected. The remaining tangential momentum dependence is discretized (see again Fig. 7). Equivalently, one can view this parametrization as a discretization of momentum dependences corresponding to a partition of the Brillouin zone in "patches" or "sectors" [35, 36].

The flow of the two-particle vertex in the ground state of the two-dimensional Hubbard model has been computed for many different model parameters t'/t and U/t (t just fixes the absolute energy scale) and densities near half-filling [35, 34, 36, 37]. In all cases the vertex develops a strong momentum dependence for small Λ with divergences for several momenta at some critical scale $\Lambda_c > 0$, which vanishes exponentially for $U \to 0$. To see which physical instability is associated with the diverging vertex function, several susceptibilities have been computed, in particular commensurate and incommensurate spin susceptibilities $\chi_S(\mathbf{q})$ with $\mathbf{q} = (\pi, \pi)$, $\mathbf{q} = (\pi - \delta, \pi)$ and $\mathbf{q} = (1 - \delta)(\pi, \pi)$, where δ is a function of density [38]; the commensurate charge susceptibility $\chi_C((\pi, \pi))$; and singlet pair susceptibilities with s-wave and d-wave form factors. Some of these susceptibilities diverge together with the vertex function at the scale Λ_c. Depending on the choice of U, t' and μ, the strongest divergence is found either for the commensurate or incommensurate spin susceptibility, or for the pairing susceptibility with $d_{x^2-y^2}$ symmetry.

Fig. 7 shows a typical result for the flow of the two-particle interactions and susceptibilities in the ground state of the two-dimensional Hubbard model, as obtained from the Wick ordered version of the functional RG [34]. Within the lowest order truncation for the two-particle vertex, the results obtained from different functional RG versions do not deviate significantly from each other. Only the singlet part of the vertex is plotted, for various choices of two incoming momenta and one outgoing momentum on the Fermi surface. The triplet part of the vertex flows generally more weakly than the singlet part. Note the threshold at $\Lambda = 2|\mu|$ below which the amplitudes for various scattering processes, especially umklapp scattering, renormalize only very slowly. The flow of the antiferromagnetic spin susceptibility is cut off at the same scale. The infinite slope singularity in some of the flows at scale $\Lambda = |\mu|$ is due to the van Hove singularity being crossed at that scale. The *pairing* susceptibility with $d_{x^2-y^2}$-symmetry diverges at the scale Λ_c, at which also the two-particle interaction diverges in the Cooper channel.

Following the flow of the vertex function and susceptibilities, one can see that those interaction processes which enhance the antiferromagnetic spin susceptibility (especially umklapp scattering) also build up an attractive interaction in the $d_{x^2-y^2}$ pairing channel. This confirms the spin-fluctuation route to d-wave superconductivity. Running the flow for various choices of μ/t and U/t one obtains an educated guess for the ground state phase diagram from the dominant divergences of the vertex and susceptibilities.

The static approximation of the vertex with a discretized momentum dependence as described above is sufficient for a weak coupling stability analysis. However, near the scale Λ_c, where the vertex diverges, this crude parametrization does not capture the momentum and energy dependence of the emerging singularities, and the power-counting argument invoked for its justification breaks down. Recently, an improved parametrization of the two-particle vertex based on an additive decomposition in charge, magnetic, and pairing channels has been established [15, 39, 40]. In this channel decomposition, singular momentum and energy dependences are isolated in a single bosonic momentum and energy variable, corresponding to a sum or difference of fermionic variables, which can then be parametrized much more accurately.

3.2   Spontaneous symmetry breaking

Within the one-loop truncation the effective two-particle interaction Γ^Λ always diverges in some momentum channels at a finite energy scale Λ_c, even for a small bare interaction U. Hence, one is always running into a strong coupling problem in the low-energy limit. The one-loop truncation breaks down, and also the simplified parametrization of the two-particle vertex described above cannot be justified in the presence of singular momentum and energy dependences.

If the vertex function diverges only in the Cooper channel, driven by the particle-particle contribution to the flow, the strong coupling problem emerging in the low-energy region can be controlled by exploiting Λ_c as a small parameter [41]. The formation of a superconducting ground state can then be described essentially by a BCS theory with renormalized input parameters. In the Hubbard model, the pure Cooper channel instability is always realized for $\mu \neq \epsilon_{\mathrm{vH}}$ at sufficiently small U. In that regime, one can safely infer superconductivity with a d-wave order parameter from the divergence of the one-loop pairing susceptibility. At finite temperature, the off-diagonal long-range order will of course turn into the quasi long-range order of a Kosterlitz-Thouless phase.

In general, the one-loop calculation can produce divergences of the vertex function in various momentum channels, with large contributions from both particle-particle and particle-hole diagrams. This can happen even in the weak coupling limit $U \to 0$, namely when the chemical potential approaches the van Hove singularity. In that case, different possible instabilities can compete in a complicated way. Besides spin density wave and pairing instabilities, one has to deal with ferromagnetism (at moderate $|t'/t|$ in the Hubbard model) [42–44] and a d-wave Pomeranchuk instability of the Fermi surface [45] as alternative or coexisting candidates.

A complete theory of the effective strong coupling problem emerging from strong particle-particle and particle-hole fluctuations has not yet been achieved. For weak bare coupling, one may again try to exploit the smallness of the scale Λ_c where strong fluctuations appear to construct a tractable effective low-energy theory. Spontaneous symmetry breaking can be handled within the functional RG framework by adding an infinitesimal symmetry breaking term at the beginning of the flow, which is then promoted to a finite order parameter at the scale Λ_c [19,20]. The calculations are complicated by the appearance of anomalous interaction vertices, and, in case of continous symmetries, by singularities associated with Goldstone modes. Nevertheless, fermionic functional RG flows with spontaneous symmetry breaking were computed for the superconducting ground state of the attractive [46,47] and repulsive [48] Hubbard model. In systems with a metastable phase, e.g., near a first order transition, a shift of the initial conditions by a counter term is needed to drive the flow into the stable symmetry broken phase [49]. Order parameter fluctuations are most conveniently treated by introducing appropriate bosonic fields, as first discussed for antiferromagnetic order in the half-filled Hubbard model [50].

In case of competing order parameters, such as antiferromagnetism and d-wave superconductivity near half-filling, a full RG treatment of spontaneous symmetry-breaking and order parameter fluctuations is a rather ambitious long-term goal [51]. As a simpler alternative one may neglect low-energy fluctuations and combine the RG with a mean-field (MF) theory of symmetry-
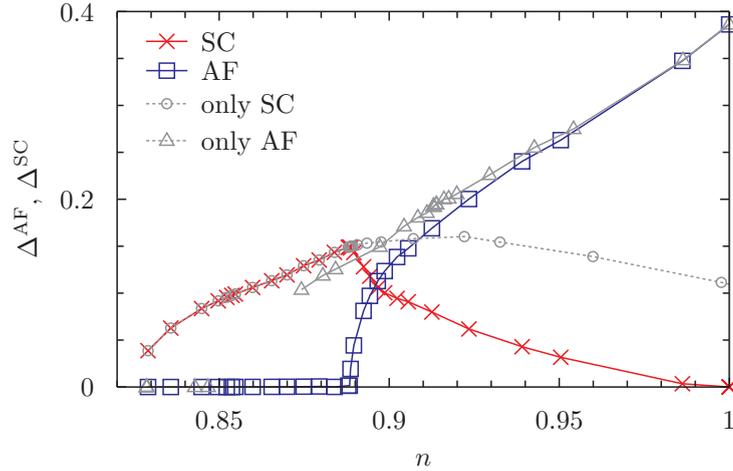
Fig. 8: *Amplitudes of antiferromagnetic and superconducting gap functions in the ground state of the two-dimensional Hubbard model as a function of density, for $U/t = 3$ and $t'/t = -0.15$. Results from a coupled solution of the magnetic and superconducting gap equations with partial coexistence of orders are compared to purely magnetic and purely superconducting solutions. The amplitudes are plotted in units of t. Figure taken from Ref. [53].*

breaking [52, 53]. In such a RG+MF approach, the one-loop flow is stopped at a scale Λ_{MF} that is small compared to the band width but still safely above the scale Λ_c where the two-particle vertex diverges. At this point the vertex has already developed a pronounced momentum dependence, reflecting in particular magnetic and superconducting correlations. The integration over the remaining modes, below Λ_{MF}, is treated in a mean-field approximation allowing, in particular, antiferromagnetic and superconducting order, where the effective interactions entering the mean-field equations are extracted from $\Gamma^{\Lambda_{\mathrm{MF}}}$. At zero temperature, this approach should yield a decent approximation for the order parameters, since order parameter fluctuations usually do not play a crucial role for the gross features of the ground state. Results obtained for the amplitudes of the antiferromagnetic and superconducting gap functions in the ground state of the 2D Hubbard model, as obtained from a functional RG + MF calculation [53], are shown in Fig. 8. The amplitudes are defined as the maxima $\Delta^{\mathrm{AF}} = \max_{\mathbf{k}} \Delta_{\mathbf{k}}^{\mathrm{AF}}$ and $\Delta^{\mathrm{SC}} = \max_{\mathbf{k}} \Delta_{\mathbf{k}}^{\mathrm{SC}}$ of the gap functions. There is an extended region of *coexistence* of magnetic and superconducting order, which occurs naturally due to pairing of electrons near the reconstructed Fermi surface (pockets) in the antiferromagnetic state. In Fig. 9, the momentum dependence of the gap functions is shown for four distinct densities at and below half-filling. The superconducting gap function has the expected d-wave symmetry, while the antiferromagnetic gap has s-wave symmetry with a relatively weak momentum dependence.

4 Leap to strong coupling: DMFT as a booster rocket

A truncation of the functional RG hierarchy of flow equations can be justified only for weak interactions, with the exception of mean-field models where phase space restrictions suppress higher order contributions [19]. Although bare interactions are usually two-particle interactions, m-particle effective interactions with $m > 2$ are generated by the flow and affect the
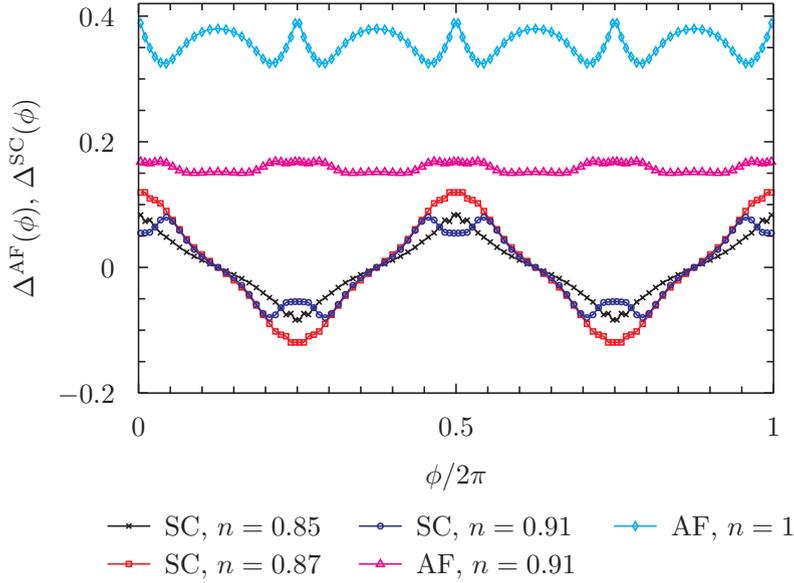
Fig. 9: *Momentum dependence of the antiferromagnetic and superconducting gap functions for various choices of the density. The momentum dependence is parametrized by the angle ϕ between $\mathbf{k}$ and the k_x-axis, where $\Delta_{\mathbf{k}}^{\text{AF}}$ is evaluated with $\mathbf{k}$ on the umklapp surface ($|k_x \pm k_y| = \pi$) and $\Delta_{\mathbf{k}}^{\text{SC}}$ with $\mathbf{k}$ on the Fermi surface. The model parameters are the same as in Fig. 8. Figure taken from Ref. [53].*

effective two-particle interaction and the self-energy. For example, an effective three-particle interaction $\Gamma^{(6)\Lambda}$ is generated by a contribution of third order in the two-particle vertex $\Gamma^{(4)\Lambda}$, which then feeds back into the flow of $\Gamma^{(4)\Lambda}$, as can be seen in Fig. 3. For strong bare interactions, these contributions from effective interactions beyond the two-particle level become important already at relatively high energy scales, that is, at scales well above the critical scales for instabilities.

For systems with short-range interactions such as the Hubbard model, the correlations at high and intermediate energy scales are well described by the dynamical mean-field theory (DMFT) and its quantum cluster extensions, since long-range correlations emerge only at low energy scales [54]. In particular, the DMFT captures non-perturbative phenomena such as the Mott-Hubbard metal-insulator transition, which is a consequence of strong local correlations [55].

The DMFT is based on a local approximation for the fermionic self-energy, which is exact in the limit of infinite lattice dimensionality [56]. In that limit, irreducible m-particle vertices are local, too. It is thus natural to use the DMFT solution as a starting point, and include non-local correlations subsequently by expanding around the DMFT vertices and self-energy [57]. Several such extensions of the DMFT, involving various types of resummed perturbation expansions for non-local corrections, have already been proposed [58–60].

Most recently, it was shown that the DMFT can be used as a non-perturbative starting point for a functional RG flow [4]. The DMFT vertices and self-energy set the initial condition of the flow. In the remainder of this section, I will describe the fusion of DMFT and functional RG to the non-perturbative DMF^2RG, and discuss first results for the two-dimensional Hubbard model.

4.1   Dynamical mean-field theory

The DMFT was developed in two steps. First, it was shown that models of interacting lattice fermions have a non-trivial infinite dimensionality $d \to \infty$ limit [56], where local correlations survive, while non-local contributions to one-particle irreducible quantities such as the self-energy vanish [56, 61]. Second, it was shown that a lattice fermion system with a local self-energy can be mapped to a quantum impurity problem with a self-consistency condition [62, 63]. The resulting equations are a dynamical variant of the static Weiss mean-field theory for magnets [62] – hence the name "dynamical mean-field theory" commonly used since 1995.

For the Hubbard model, the DMFT equations can be derived on the back of an envelope as follows. The propagator G is related to the bare propagator G_0 and the self-energy Σ by Dyson's equation, $G^{-1}(k_0, \mathbf{k}) = G_0^{-1}(k_0, \mathbf{k}) - \Sigma(k_0)$. Non-local (in real space) contributions to the self-energy are discarded in the DMFT, so that $\Sigma(k)$ depends only on frequency. This approximation becomes exact in the limit $d \to \infty$ [56, 61]. In a one-particle irreducible skeleton expansion, the local part of the self-energy is a functional of the local propagator

$$G_{\mathrm{loc}}(k_0) = \int_{\mathbf{k}} G(k_0, \mathbf{k}) \; , \tag{42}$$

where $\int_{\mathbf{k}} = \int \frac{d^d \mathbf{k}}{(2\pi)^d}$. The same skeleton expansion yields the self-energy of the purely local action

$$\mathcal{S}_{\mathrm{loc}}[\psi, \bar{\psi}] = - \sum_{k_0, \sigma} \bar{\psi}_{k_0, \sigma} \mathcal{G}_0^{-1}(k_0) \psi_{k_0, \sigma} + U \int_0^{\beta} d\tau \, \bar{\psi}_{\uparrow}(\tau) \psi_{\uparrow}(\tau) \bar{\psi}_{\downarrow}(\tau) \psi_{\downarrow}(\tau) \; , \tag{43}$$

where τ denotes imaginary time and $\psi_{\sigma}(\tau)$ and $\bar{\psi}_{\sigma}(\tau)$ are the Fourier transforms of $\psi_{k_0, \sigma}$ and $\bar{\psi}_{k_0, \sigma}$, respectively. The dynamical *Weiss field* $\mathcal{G}_0^{-1}$ is determined by the self-consistency condition requiring that the local propagator and the self-energy of the lattice electrons coincide with the propagator and the self-energy of $\mathcal{S}_{\mathrm{loc}}$, that is,

$$G_{\mathrm{loc}}^{-1}(k_0) = \mathcal{G}_0^{-1}(k_0) - \Sigma(k_0) \; . \tag{44}$$

The main difficulty is to compute the self-energy as a functional of $\mathcal{G}_0$ from the action $\mathcal{S}_{\mathrm{loc}}$. Introducing an auxiliary bath of non-interacting conduction electrons, this problem can be mapped to a well-known quantum impurity problem, the single-impurity Anderson model [62, 63], for which efficient non-perturbative numerical algorithms exist. Once a self-consistent $\mathcal{G}_0$ has been determined, one can also compute DMFT vertices from $\mathcal{S}_{\mathrm{loc}}$ [64].

4.2   From infinite to finite dimensions

We now set up a flow which starts from the local self-energy and local vertices as given by the DMFT, and builds up non-local correlations successively [4]. Without truncations, the exact non-local quantities would be obtained at the end of the flow. There is no double-counting of contributions. One way of defining such a flow, which is associated with an intuitive picture, is
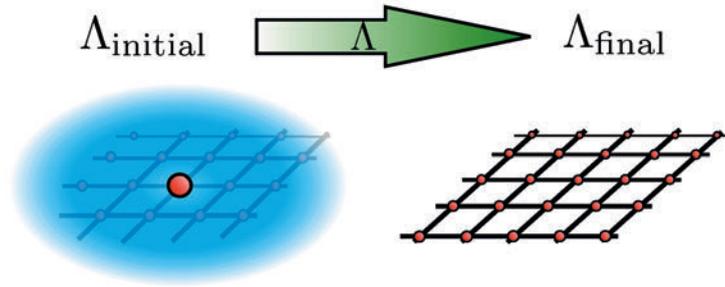
Fig. 10: *Illustration of the flow from a DMFT solution to the solution of the d-dimensional (here $d = 2$) lattice system. Figure taken from Ref. [4].*

to flow from infinite dimensions, where the DMFT is exact, to the actual dimensionality of the system.

To be specific, let us consider a d-dimensional hypercubic lattice with nearest neighbor hopping, supplemented by $\bar{d}$ additional auxiliary dimensions with $\bar{d} \to \infty$. The flow equations derived in Sec. 2 are valid for an arbitrary scale dependence of the bare propagator. To flow from infinite to d dimensions, we introduce scale dependent hopping amplitudes in the physical and auxiliary directions, denoted by t^Λ and $\bar{t}^\Lambda$, respectively. The initial hopping amplitudes are $t^{\Lambda_0} = 0$ and $\bar{t}^{\Lambda_0} = (d/\bar{d})^{1/2}\, t$. The scaling with $\bar{d}^{-1/2}$ is required for a proper limit $\bar{d} \to \infty$ [56]. At the end of the flow, for $\Lambda \to 0$, the hopping amplitude in the auxiliary dimensions are switched off, $\bar{t}^{\Lambda \to 0} = 0$, while the real hopping amplitude is turned on, $t^{\Lambda \to 0} = t$.

The corresponding scale dependent bare propagator has the form

$$G_0^\Lambda(k_0, \mathbf{k}, \bar{\mathbf{k}}) = \frac{1}{ik_0 + \mu - \epsilon_\mathbf{k}^\Lambda - \bar{\epsilon}_{\bar{\mathbf{k}}}^\Lambda}\,, \tag{45}$$

with the scale dependent dispersion relations

$$\begin{aligned}
\epsilon_\mathbf{k}^\Lambda &= -2t^\Lambda \left(\cos k_1 + \cdots + \cos k_d\right)\,, \\
\bar{\epsilon}_{\bar{\mathbf{k}}}^\Lambda &= -2\bar{t}^\Lambda \left(\cos \bar{k}_1 + \cdots + \cos \bar{k}_{\bar{d}}\right)\,.
\end{aligned} \tag{46}$$

For $\bar{d} \to \infty$, only the part of the propagator which is local in the auxiliary dimensions contributes to the self-energy and vertices. That local part is given by a $\bar{\mathbf{k}}$-integration,

$$G_0^\Lambda(k_0, \mathbf{k}) = \int_{\bar{\mathbf{k}}} G_0^\Lambda(k_0, \mathbf{k}, \bar{\mathbf{k}}) = \int d\bar{\epsilon}\, \frac{\bar{\rho}^\Lambda(\bar{\epsilon})}{ik_0 + \mu - \epsilon_\mathbf{k}^\Lambda - \bar{\epsilon}}\,, \tag{47}$$

where $\bar{\rho}^\Lambda(\bar{\epsilon})$ is the density of states for $\bar{\epsilon}_{\bar{\mathbf{k}}}^\Lambda$. The latter is a normalized Gaussian distribution with a width that shrinks to zero for $\Lambda \to 0$, so that $G_0^{\Lambda \to 0}(k_0, \mathbf{k}) = (ik_0 + \mu - \epsilon_\mathbf{k})^{-1}$.

G_0^Λ defines a flow that interpolates smoothly between the DMFT solution for the infinite dimensional model at Λ_0 and the solution of the d-dimensional system for $\Lambda \to 0$, as illustrated schematically in Fig. 10. The flow equations derived in Sec. 2 apply without any modification. However, the initial condition for the flow is not given by bare quantities, but by the self-energy

$$\frac{d}{d\Lambda} \Sigma^\Lambda = \quad \text{(diagram with } S^\Lambda, \Gamma^\Lambda) \qquad\qquad \frac{d}{d\Lambda} \Gamma^\Lambda = \quad \text{(diagram with } S^\Lambda, G^\Lambda)$$

Fig. 11: *Truncation of flow equations in* $\mathrm{DMF^2RG}$ *applied to the 2D Hubbard model.*

and vertices as obtained from the DMFT, that is, $\Sigma^{\Lambda_0} = \Sigma_{\mathrm{DMFT}}$ and $\Gamma^{(2m)\Lambda_0} = \Gamma^{(2m)}_{\mathrm{DMFT}}$. Hence, non-perturbative local correlations effects, such as the Mott-Hubbard transition, are built in already at the starting point. The DMFT thus becomes a "booster rocket" for the flow.

The infinite dimensionality limit served as a guide to develop the idea of setting up a flow that starts with the DMFT. However, the DMFT is usually applied as an approximation for a finite dimensional system, without introducing extra dimensions. In the same spirit, one can also define a flow with the DMFT as a starting point, while staying entirely in the d-dimensional physical space. A particularly simple choice for the scale dependence of the bare propagator is given by [4]

$$\left[G_0^\Lambda(k_0, \mathbf{k}) \right]^{-1} = \Lambda \, \mathcal{G}_0^{-1}(k_0) + (1 - \Lambda) \, G_0^{-1}(k_0, \mathbf{k}) , \tag{48}$$

with $\Lambda_0 = 1$. This choice is very simple but certainly not optimal. In particular, it does not regularize infrared singularities. Better choices obeying additional requirements besides the correct boundary conditions can be constructed on demand.

4.3   Application to the 2D Hubbard model

Since the $\mathrm{DMF^2RG}$ has been proposed very recently, there is only one concrete application, for the two-dimensional Hubbard model with pure nearest neighbor hopping at half-filling [4]. Due to perfect nesting, the ground state is antiferromagnetically ordered for any $U > 0$ in that case. In that first application, relativly crude approximations were made to compute the flow. The calculation was done directly in two dimensions, with the DMFT solution as starting point, and the flow was defined by G_0^Λ as in Eq. (48). The flow was truncated by discarding $\Gamma^{(6)\Lambda}$, such that $\Gamma^\Lambda = \Gamma^{(4)\Lambda}$ and Σ^Λ are determined by a closed system of one-loop flow equations, see Fig. 11, with the DMFT self-energy Σ_{DMFT} and two-particle vertex Γ_{DMFT} as initial condition. The rationale behind this truncation is that the strongest local correlations are already included by the DMFT starting point, and that the effect of three-particle correlations on non-local correlations can be expected to be less important. Clearly, this needs to be checked in the future. The frequency dependence of the vertex was parametrized by using a channel decomposition as in Refs. [15, 40] with only one important frequency dependence in each channel. The latter can be discretized accurately, as can the frequency dependence of the self-energy. However, the channel decomposition does not capture certain structures appearing in the DMFT vertex
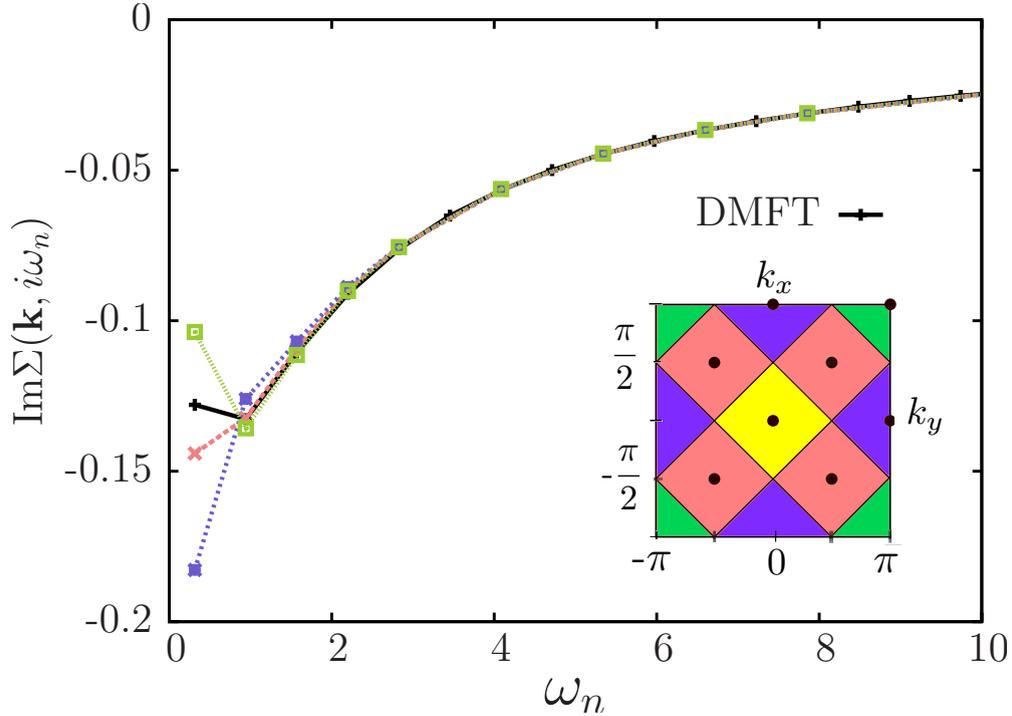
Fig. 12: *Imaginary part of the fermionic self-energy as a function of Matsubara frequency for the half-filled 2D Hubbard model at $U = 4t$ and $T = 0.4t$. The DMFT result ($\mathbf{k}$-independent) is compared to the result from the $\mathrm{DMF^2RG}$, where the color coding of $\mathbf{k}$ is defined in the inset. Note that the results for $\mathbf{k} = (0,0)$ and $\mathbf{k} = (\pi, \pi)$ coincide due to particle-hole symmetry. Figure taken from Ref. [4].*

at strong coupling [64], which limited the calculations to interaction strengths below the Mott insulator regime. The momentum dependence was discretized with a few patches.

A result for the self-energy of the half-filled 2D Hubbard model obtained from the $\mathrm{DMF^2RG}$ as described above is shown in Fig. 12, and compared to the DMFT solution. The discretization of momentum space is shown in the inset. A relatively high temperature $T = 0.4t$ was chosen so that the flow could be carried out until $\Lambda = 0$ without running into divergences associated with the antiferromagnetic instability. The $\mathrm{DMF^2RG}$ result deviates significantly from the momentum independent DMFT solution only at the lowest Matsubara frequencies. There, a pronounced momentum dependence emerges. The trend of a large enhancement of the self-energy at momenta near $(\pi, 0)$ and $(0, \pi)$, related to a pseudogap formation, agrees with results from cluster extensions of the DMFT [65]. The results also agree qualitatively with those obtained from a plain one-loop functional RG calculation, confirming that a weak coupling expansion is still reasonable at moderate coupling strengths as $U = 4t$. Clearly, qualitative differences between weak-coupling truncations of the functional RG and the non-perturbative $\mathrm{DMF^2RG}$ are to be expected at interaction strengths comparable to the band width and beyond. To apply the $\mathrm{DMF^2RG}$ at large U, a suitable parametrization of the complex frequency and momentum dependence of the two-particle vertex at strong coupling needs to be developed.

5   Conclusion

The functional RG has become a valuable source of new approximation schemes for interacting Fermi systems [3]. The method is based on an exact flow equation, which describes the flow of the effective action as a function of a suitable flow parameter. From the final effective action, at the end of the flow, any desired information about the system can be obtained. Approximations are constructed by truncating the effective action. In many cases, rather simple truncations turned out to capture rather complex many-body phenomena. Compared to the traditional resummations of perturbation theory, these approximations have the advantage that infrared singularities are treated properly due to the built-in RG structure. Unlike other RG methods, approximations derived in the functional RG framework can be applied directly to microscopic models, not only to renormalizable effective field theories. Remarkably, the functional RG reviewed here as a computational tool is very similar to RG approaches used by mathematicians to derive general rigorous results for interacting Fermi systems.

Applications of the functional RG to the two-dimensional Hubbard model have improved our understanding of its instabilities. In particular, the existence of d-wave superconductivity in that model was conclusively established.

With the very recent fusion of DMFT and functional RG [4], where the DMFT is used as a non-perturbative starting point for the functional RG flow, a promising route has been opened to capture all aspects of strongly interacting Fermi systems, such as the 2D Hubbard model at large U, over all energy scales in one framework.

Acknowledgment

Appendix

A   Derivation of functional flow equation

Here we describe the derivation of the functional flow equation (15) for the effective action Γ^Λ. Introducing a scale-dependent bare propagator $G_0^\Lambda = (Q_0^\Lambda)^{-1}$ in the functional integral representation (4) of the generating functional for connected Green functions, one can write

$$e^{-\mathcal{G}^\Lambda[\eta,\bar\eta]} = \int \prod_K d\psi_K d\bar\psi_K \, e^{(\bar\psi, Q_0^\Lambda \psi)} \, e^{-V[\psi,\bar\psi]} \, e^{(\bar\eta,\psi)+(\bar\psi,\eta)} \ . \tag{49}$$

Taking a Λ-derivative on both sides yields

$$
\begin{aligned}
-(\partial_\Lambda \mathcal{G}^\Lambda[\eta,\bar\eta]) \, e^{-\mathcal{G}^\Lambda[\eta,\bar\eta]} &= \int \prod_K d\psi_K d\bar\psi_K \, (\bar\psi, \partial_\Lambda Q_0^\Lambda \psi) \, e^{(\bar\psi, Q_0^\Lambda \psi)} \, e^{-V[\psi,\bar\psi]} \, e^{(\bar\eta,\psi)+(\bar\psi,\eta)} \\
&= -(\partial_\eta, \partial_\Lambda Q_0^\Lambda \partial_{\bar\eta}) \, e^{-\mathcal{G}^\Lambda[\eta,\bar\eta]} \ ,
\end{aligned}
\tag{50}
$$

which leads directly to a flow equation for $\mathcal{G}^\Lambda$,

$$\frac{d}{d\Lambda} \, \mathcal{G}^\Lambda[\eta,\bar\eta] = \left(\frac{\partial \mathcal{G}^\Lambda}{\partial\eta}, \frac{dQ_0^\Lambda}{d\Lambda} \frac{\partial \mathcal{G}^\Lambda}{\partial\bar\eta} \right) + \mathrm{Tr}\left(\frac{dQ_0^\Lambda}{d\Lambda} \frac{\partial^2 \mathcal{G}^\Lambda}{\partial\bar\eta \partial\eta} \right) \ . \tag{51}$$

The effective action is the Legendre transform

$$\Gamma^\Lambda[\psi,\bar\psi] = \mathcal{G}^\Lambda[\eta^\Lambda, \bar\eta^\Lambda] + (\bar\psi, \eta^\Lambda) + (\bar\eta^\Lambda, \psi) \ . \tag{52}$$

Note that η^Λ and $\bar\eta^\Lambda$ are Λ-dependent functions of ψ and $\bar\psi$, so that

$$\frac{d}{d\Lambda} \, \Gamma^\Lambda[\psi,\bar\psi] = \frac{d}{d\Lambda} \, \mathcal{G}^\Lambda[\eta^\Lambda, \bar\eta^\Lambda] + (\bar\psi, \partial_\Lambda \eta^\Lambda) + (\partial_\Lambda \bar\eta^\Lambda, \psi) \ . \tag{53}$$

The total derivative acts also on the Λ-dependence of η^Λ and $\bar\eta^\Lambda$. Using the relations $\partial\mathcal{G}^\Lambda/\partial\bar\eta = -\psi$, and $\partial\mathcal{G}^\Lambda/\partial\eta = \bar\psi$, all terms arising from the Λ-dependence of η^Λ and $\bar\eta^\Lambda$ cancel, yielding

$$\frac{d}{d\Lambda} \, \Gamma^\Lambda[\psi,\bar\psi] = \frac{d}{d\Lambda} \, \mathcal{G}^\Lambda[\eta^\Lambda, \bar\eta^\Lambda]\bigg|_{\eta^\Lambda, \bar\eta^\Lambda \text{ fixed}} \ . \tag{54}$$

The flow equation (15) for Γ^Λ now follows directly from Eq. (51) and the reciprocity relation $\mathbf{\Gamma}^{(2)\Lambda}[\psi,\bar\psi] = \left(\mathbf{G}^{(2)\Lambda}[\eta^\Lambda, \bar\eta^\Lambda] \right)^{-1}$.

References

[1] J. Berges, N. Tetradis, and C. Wetterich, Phys. Rep. **363**, 223 (2002)

[2] P. Kopietz, L. Bartosch, and F. Schütz:
Introduction to the Functional Renormalization Group (Springer, Berlin, 2010).

[3] W. Metzner, M. Salmhofer, C. Honerkamp, V. Meden, and K. Schönhammer,
Rev. Mod. Phys. **84**, 299 (2012)

[4] C. Taranto, S. Andergassen, J. Bauer, K. Held, A.A. Katanin, W. Metzner, G. Rohringer,
and A. Toschi, Phys. Rev. Lett. **112**, 196402 (2014)

[5] J. Solyom, Adv. Phys. **28**, 201 (1979)

[6] J. Feldman and E. Trubowitz, Helv. Phys. Acta **63**, 156 (1990); *ibid* **64**, 214 (1991)

[7] G. Benfatto and G. Gallavotti, J. Stat. Phys. **59**, 541 (1990)

[8] K.G. Wilson and J. Kogut, Phys. Rep. C **12**, 75 (1974)

[9] M. Salmhofer: *Renormalization: An Introduction* (Springer, Heidelberg, 1999)

[10] J. Feldman, H. Knörrer, and E. Trubowitz, Rev. Math. Phys. **15**, 949-1169 (2003);
Commun. Math. Phys. **247**, 1-320 (2004)

[11] R. Shankar, Rev. Mod. Phys. **66**, 129 (1994)

[12] J. Polchinski, in *Proceedings of 1993 Theoretical Advanced Studies Institute in Elementary Particle Physics*, ed. by J. Harvey, J. Polchinski (World Scientific, Singapore, 1993)

[13] C. Wetterich, Phys. Lett. B **301**, 90 (1993)

[14] J.W. Negele and H. Orland, *Quantum Many-Particle Systems*
(Addison-Wesley, Reading, 1987)

[15] C. Husemann and M. Salmhofer, Phys. Rev. B **79**, 195125 (2009)

[16] S. Andergassen, T. Enss, V. Meden, W. Metzner, U. Schollwöck, and K. Schönhammer,
Phys. Rev. B **70**, 075102 (2004)

[17] J. Polchinski, Nucl. Phys. **B231**, 269 (1984)

[18] F. Schütz, L. Bartosch, and P. Kopietz, Phys. Rev. B **72**, 035107 (2005)

[19] M. Salmhofer, C. Honerkamp, W. Metzner, and O. Lauscher,
Prog. Theor. Phys. **112**, 943 (2004)

[20] R. Gersch, C. Honerkamp, D. Rohe, and W. Metzner, Eur. Phys. J. B **48**, 349 (2005)

[21] A. Eberlein and W. Metzner, Prog. Theor. Phys. **124**, 471 (2010)

[22] M. Salmhofer and C. Honerkamp, Prog. Theor. Phys. **105**, 1 (2001)

[23] P.W. Anderson, Science **235**, 1196 (1987)

[24] For an early review on d-wave superconductivity from spin fluctuations, see
D.J. Scalapino, Phys. Rep. **250**, 329 (1995)

[25] K. Miyake, S. Schmitt-Rink, and C.M. Varma, Phys. Rev. B **34**, 6554 (1986)

[26] D.J. Scalapino, E. Loh, and J.E. Hirsch, Phys. Rev. B **34**, 8190 (1986)

[27] N.E. Bickers, D.J. Scalapino, and R.T. Scalettar, Int. J. Mod. Phys. B **1**, 687 (1987)

[28] N.E. Bickers, D.J. Scalapino, and S.R. White, Phys. Rev. Lett. **62**, 961 (1989)

[29] D. Manske: *Theory of Unconventional Superconductors*,
Springer Tracts in Modern Physics, vol. 202 (Springer, Berlin, 2004)

[30] For reviews of numerical work, see E. Dagotto, Rev. Mod. Phys. **66**, 763 (1994);
N. Bulut, Adv. Phys. **51**, 1587 (2002)

[31] H.J. Schulz, Europhys. Lett. **4**, 609 (1987)

[32] I. Dzyaloshinskii, Sov. Phys. JETP **66**, 848 (1987)

[33] P. Lederer, G. Montambaux, and D. Poilblanc, J. Phys. (Paris) **48**, 1613 (1987)

[34] C.J. Halboth and W. Metzner, Phys. Rev. B **61**, 7364 (2000)

[35] D. Zanchi and H.J. Schulz, Europhys. Lett. **44**, 235 (1998); Phys. Rev. B **61**, 13609 (2000)

[36] C. Honerkamp, M. Salmhofer, N. Furukawa, and T.M. Rice,
Phys. Rev. B **63**, 035109 (2001)

[37] A.P. Kampf and A.A. Katanin, Phys. Rev. B **67**, 125104 (2003)

[38] See, for example, H.J. Schulz, Phys. Rev. Lett. **64**, 1445 (1990), where also the choice of
δ as a function of doping is discussed.

[39] C. Husemann, K.-U. Giering, and M. Salmhofer, Phys. Rev. B **85**, 075121 (2012)

[40] A similar channel decomposition was derived and applied also for the single-impurity
Anderson model by C. Karrasch, R. Hedden, R. Peters, T. Pruschke, K. Schönhammer,
and V. Meden, J. Phys. Condens. Matter **20**, 345205 (2008)

[41] J. Feldman, J. Magnen, V. Rivasseau, and E. Trubowitz, Europhys. Lett. **24**, 437 (1993)

[42] R. Hlubina, S. Sorella, and F. Guinea, Phys. Rev. Lett. **78**, 1343 (1997)

[43] C. Honerkamp and M. Salmhofer, Phys. Rev. Lett. **87**, 187004 (2001)

[44] A.A. Katanin and A.P. Kampf, Phys. Rev. B **68**, 195101 (2003)

[45] C.J. Halboth and W. Metzner, Phys. Rev. Lett. **85**, 5162 (2000)

[46] R. Gersch, C. Honerkamp, and W. Metzner, New J. Phys. **10**, 045003 (2008)

[47] A. Eberlein and W. Metzner, Phys. Rev. B **87**, 174523 (2013)

[48] A. Eberlein and W. Metzner, Phys. Rev. B **89**, 035126 (2014)

[49] R. Gersch, J. Reiss, and C. Honerkamp, New J. Phys. **8**, 320 (2006)

[50] T. Baier, E. Bick, and C. Wetterich, Phys. Rev. B **70**, 125111 (2004)

[51] S. Friederich, H. C. Krahl, and C. Wetterich, Phys. Rev. B **81**, 235108 (2010);
ibid. **83**, 155125 (2011)

[52] J. Reiss, D. Rohe, and W. Metzner, Phys. Rev. B **75**, 075110 (2007)

[53] J. Wang, A. Eberlein, and W. Metzner, Phys. Rev. B **89**, 121116(R) (2014)

[54] A. Georges, Ann. Phys. (Berlin) **523**, 672 (2011)

[55] A. Georges, G. Kotliar, W. Krauth, and M. Rozenberg, Rev. Mod. Phys. **68**, 13 (1996)

[56] W. Metzner and D. Vollhardt, Phys. Rev. Lett. **62**, 324 (1989)

[57] Within the Gutzwiller variational ansatz, a perturbative expansion for non-local corrections around the local $d = \infty$ solution was shown to be very promising already long ago, see W. Metzner, Z. Phys. **77**, 253 (1989)

[58] J.P. Hague, M. Jarrell, and T.C. Schulthess, Phys. Rev. B **69**, 165113 (2004)

[59] A. Toschi, A.A. Katanin, and K. Held, Phys. Rev. B **75**, 045118 (2007); A. Valli, G. Sangiovanni, O. Gunnarsson, A. Toschi, and K. Held, Phys. Rev. Lett. **104**, 246402 (2010); G. Rohringer, A. Toschi, A.A. Katanin, and K. Held, Phys. Rev. Lett. **107**, 256402 (2011)

[60] A.N. Rubtsov, M.I. Katsnelson, and A.I. Lichtenstein, Phys. Rev. B **77**, 033101 (2008); H. Hafermann, G. Li, A.N. Rubtsov, M.I. Katsnelson, A.I. Lichtenstein, and H. Monien, Phys. Rev. Lett. **102**, 206401 (2009)

[61] E. Müller-Hartmann, Z. Phys. B **74**, 507 (1989); *ibid.* **76**, 211 (1989).

[62] A. Georges and G. Kotliar, Phys. Rev. B **45**, 6479 (1992)

[63] M. Jarrell, Phys. Rev. Lett. **69**, 168 (1992)

[64] For a comprehensive recent analysis of the two-particle vertex obtained by DMFT, see G. Rohringer, A. Valli, and A. Toschi, Phys. Rev. B **86**, 125114 (2012)

[65] T.A. Maier, M. Jarrell, T. Pruschke, and M.H. Hettler, Rev. Mod. Phys. **77**, 1027 (2005)